Eur. Phys. J. D **59**, 379–387 (2010)
DOI: 10.1140/epjd/e2010-00140-6

THE EUROPEAN PHYSICAL JOURNAL D

Regular Article

Complex scattering potential – ionization contribution (CSP-ic) method for calculating total ionization cross sections on electron impact

M. Vinodkumar[1,a], K. Korot[2], and P.C. Vinodkumar[3]

[1] V.P. & R.P.T.P. Science College, Vallabh Vidyanagar, 388 120 Gujarat, India
[2] Department of Physics, Faculty of Engineering & Technology, CHARUSAT, Changa, 388 421 Gujarat, India
[3] Department of Physics, S.P. University, Vallabh Vidyanagar, 388 120 Gujarat, India

Received 3 March 2010 / Received in final form 15 April 2010
Published online 19 May 2010 –

Abstract. In this article, we report calculations of total ionization cross sections, Q_{ion}, for simple atoms (C, N, O, F) and molecules (NO and NH_3) of atmospheric interest on electron impact at energies from threshold to 2000 eV. We have employed the complex scattering potential – ionization contribution (CSP-ic) method for the present study. Attempt has been made to improve the method by computing the parameter that involves the ratio of sum of the total excitation cross sections (ΣQ_{exc}) and total inelastic cross section (Q_{inel}) at the peak of the inelastic cross section. The present study not only provided a better estimation of the parameter involved in the CSP-ic method but also provided better agreement with the available experimental and theoretical data on the ionization cross sections of the simple atomic and molecular targets studied here.

1 Introduction

The persistent interest in the investigation of the electron atom/molecule interactions is driven by the increase in importance of the electron assisted processes in the development of modern technologies [1]. Apart from the importance of the scattering data in various applied fields they are also of fundamental theoretical importance as scattering is one of the most fundamental processes to study the structure and properties of the target. Scattering of electron gives rise to many processes of which electron induced ionization is the most important. The cross sections resulting due to electron impact ionization have been measured and calculated since the early days of collision physics because of their many fold applications in various branches of pure and applied sciences [2]. To name few, the cross section is pivotal in low temperature plasma processing, fusion edge plasma, gas discharges, modeling of planetary, stellar and cometary atmospheres, radiation chemistry, mass spectrometry, chemical analysis, medical research, etc. Demand of reliable ionization cross sections of specific atoms and molecules is ever increasing since they are the key ingredients for modeling of fusion plasma in tokamaks, modeling of radiation effects for both materials and medical research. Thus, generating the ionization cross section data through experiments as well as theory are of great interest in recent times.

[a] e-mail: minaxivinod@yahoo.co.in

Numerous measurements of electron impact ionization cross sections are reported by many groups [3–10]. Considerable progress in the experimental determination of ionization cross sections for atomic and molecular targets [11–13] have been achieved in past decades. Even though there is much advancement in experimental measurements for both total and partial ionization cross sections of various species, accurate data for most of the species over a wide electron energy range are still not available. Most of the ionization cross sections have relative uncertainties in measurements ranging from 6% to 15% [3–13]. Certain highly reactive targets, e.g. radicals and exotic systems, pose difficulties in performing the experiments and hence theoretical investigation becomes necessary.

The quantum mechanical calculations of total angle-integrated electron impact ionization cross sections are difficult, if not impossible, even for simplest atoms. Though rigorous calculations for molecular targets are difficult, complicated and in many cases beyond the capability of current quantum mechanical electron collision theory [14], advanced close-coupling calculations for electron-impact ionization of neutral atoms have been attempted [15]. However, number of approximate and semi empirical methods have been devised. The simplest is the additivity rule which derives the total ionization cross sections as sum of atomic cross sections of individual atoms forming the molecule either with or without considering molecular bonding. The additivity rule was modified and

renamed as modified additivity rule by Deustch and co-workers [14] that includes appropriately chosen weighing factors to account for molecular bonding. Besides additivity approach, Bobeldijk and co-workers [16] utilized simple geometrical approach and evaluated ionization cross sections by averaging over all possible orientations. Khare and co-workers [17] have developed a method which combines the Mott and Bethe cross sections describing ionizing collisions that occur at small and large impact parameters. The more widely employed binary-encounter-Bethe (BEB) theory developed by Kim and Rudd [18] combines the binary encounter and Bethe cross sections and introduces the additivity concept with quantum mechanically calculated molecular quantities. DM formalism and BEB formalism are 'more rigorous' theoretical approaches and they make use of an additivity concept by summing up the contributions arising from the ejection of electrons from different molecular orbitals.

Another successful theoretical model is the 'complex scattering potential – ionization contribution' called 'CSP-ic' method, a semi empirical method developed by our group [19–25]. This method has been extensively employed to extract the ionization contribution from the total inelastic cross section for varieties of targets from atoms to molecules and radicals at incident electron energies beyond the ionization threshold of the target to few thousands of eV [19–25]. It has originated from the fundamental information that the two most important constituents of total inelastic cross sections in the above energy range are the total ionization cross sections (Q_{ion}) and sum of the all total excitation cross sections (ΣQ_{exc}). This separation becomes possible as both the cross sections are purely dependent on the target properties such as ionization threshold (I) and first excitation energy (E_1) and the energy of incident projectile (E_i). The procedure to extract the ionization cross section using the CSP-ic method requires the ratio of the total ionization cross section to the inelastic cross section at the peak of the inelastic cross section (R_P) as one of the input. This ratio taken in most of the cases studied so far lies in the range 0.7 to 0.8 [19–25]. Though it provides better and fast computation of the ionization cross section for several targets studied so far, the CSP-ic method lacks sufficient physical basis particularly against the choice of the ratio at the peak of the inelastic cross section (R_P). In this paper, we make an attempt to compute the ratio R_P using the electronic excitation properties of the target. Such an attempt is warranted for this model as it is found to work well for most of the targets studied so far [19–25]. This improved CSP-ic method (ICSP-ic) is employed here to compute the total ionization cross sections for simple but important atoms like C, N, O, F and molecules like NO and NH_3.

Among the targets of present interest, carbon, nitrogen and oxygen are important constituents of the atmosphere. The data on electron impact ionization of atmospheric atoms are obviously of great interest for atmospheric physics and for related applications such as telecommunications and space-vehicle re-entry. They are also important in plasma chemistry and they are of direct relevance to the contamination of nuclear fusion devices by impurity elements such as C and O [26]. Fluorine is used for plasma etching in semiconductor manufacturing, flat panel display production and MEMS (micro-electro-mechanical system) fabrications [27]. Nitrogen oxide (NO) is a minor but significant neutral constituent of thermosphere [11]. Electron scattering study from NO plays an important role in atmospheric sciences, in particular, the catalytic destruction of ozone and in auroral display [28]. Ammonia is present in cometary, planetary and astrophysical atmospheres. It is also used as a carrier gas for the generation of various low temperature plasmas.

Thus, the total ionization cross sections on electron impact for these atoms and molecules are important in many scientific and technological applications and hence are studied over a wide energy range both theoretically and experimentally. We list in Table 1, the energy range and the methods adopted in some of the works available in literature. In the next section, we briefly review the CSP-ic method and discuss theoretical estimation of the total excitation cross section and hence the ratio R_P.

2 Theoretical methodology and ICSP-ic method

Electron atom/molecule scattering phenomenon results into elastic and inelastic processes depending on the complex nature of the interaction potential. The total inelastic cross sections are the result of complex nature of the interaction potential accounted by the absorption potential. From the theoretical point of view, the variety of open channels demand the use of approaches based on complex optical potential, giving results which could be strongly dependent on the potentials chosen [39]. Here we assume that the fixed-nuclei approximation is valid in the energy regime of present interest and interaction of electron atom/molecule system can be accordingly represented by a complex optical potential, given by,

$$V_{opt}\left(E_i, r\right) = V_R\left(E_i, r\right) + iV_I\left(E_i, r\right) \tag{1}$$

where the real part V_R comprises of static potential (V_{st}), exchange potential (V_{ex}), and polarization potential (V_p). The static potential (V_{st}) is calculated at the Hartree-Fock level. The exchange potential (V_{ex}) term accounts for electron exchange interaction between the incoming projectile and target. The polarization potential (V_p) represents approximately the short range correlation and long range polarization effect arising due to the momentary redistribution of target charge cloud. Note that the spherical complex optical potential (SCOP) as such does not require any fitting parameters. The most important basic input for evaluating all these potentials is the charge density of the target. We have used atomic charge density derived from the Hartree Fock wave functions of Bunge et al. [40]. The e–molecule system is more complex as compared to e–atom system. The complexity is reduced by adopting a single center approach [24] so as to make the spherical

Table 1. List of previous work of the ionization cross section on electron impact for the present targets and the method adopted for the study.

Target	Energy range (in eV)#	References	
		Experimental/Theoretical	Method
C	Th – 1000	Brook et al. [7]	Fast atom beam technique
	Th – 5000	*Kim and Desclaux [29,30]	BEB theory
	Th – 1000	*McGuire [31]	One-electron common-central-potential unrelaxed-core Approx.
	Th – 10000	*Bell et al. [32]	Recommended data
N	Th – 1000	Brook et al. [7]	Fast atom beam technique
	Th – 5000	*Kim and Desclaux [29,30]	BEB theory
	Th – 1000	*McGuire [31]	One-electron common-central-potential unrelaxed-core Approx.
	15 – 1100	*Rong-Mei et al. [33]	An equivalent-local optical model
O	Th – 1000	Brook et al. [7]	Fast atom beam technique
	Th – 2000	Thompson et al. [8]	Pulsed crossed beam technique
	40 – 300	Zipf [9]	Cross beam technique
	Th – 5000	*Kim and Desclaux [29,30]	BEB theory
	Th – 1000	*McGuire [31]	One-electron common-central-potential unrelaxed-core Approx.
	Th – 10000	*Bell et al. [32]	Recommended data
F	Th – 200	Hayes et al. [4]	Crossed-electron-beam-fast-atom-beam method
	Th – 200	*Margreiter et al. [34]	DM formalism
	Th – 2000	*Joshipura and Limbachiya [35]	CSP-ic
NO	Th – 1000	Rapp and Englander-Golden [5]	Self-consistent technique
	Th – 1000	Iga et al. [10]	Relative flow technique
	Th – 5000	*Hwang et al. [29,36]	BEB theory
	Th – 1000	Lindsay et al. [11]	Time-of-flight mass spectrometer
	Th – 200	Lopez et al. [12]	Fast-neutral-beam technique
	Th – 2000	*Joshipura et al. [37]	CSP-ic
NH_3	Th – 1000	Rao and Srivastava [3]	Crossed-beams apparatus
	Th – 1000	Rejoub et al. [13]	Time-of-flight mass spectrometer
	Th – 200	Märk et al. [6]	Double focusing massspectrometer
	Th – 5000	*Hwang et al. [29,36]	BEB theory
	Th – 200	*Deutsch et al. [38]	DM formalism

*Theoretical work, # Th – ionization threshold energy.

approximation applicable. For example, in case of NH_3, we reduce the system to single center by expanding the charge density of lighter hydrogen atoms at the center of heavier nitrogen atom by employing the Bessel function expansion given in Gradshetyn and Ryzhik [41]. While in the case of NO, the charge density of the constituent atoms is expanded at the center of mass of the system. The spherically averaged molecular charge-density $\rho(r)$, is determined from the constituent atomic charge density using Hartree Fock wave functions of Bunge et al. [40]. The molecular charge density $\rho(r)$, so obtained is renormalized to incorporate the covalent bonding [22]. In the SCOP method, the spherical part of the complex optical potential is treated exactly in a partial wave analysis to yield various cross sections [42]. Here we have neglected the non spherical terms arising from the vibrational and rotational excitation in the full expansion of the optical potential when applied to molecules as their contribution to the inelastic channel will be low at the intermediate and high energies of present interest [42].

As our interest is to extract the total ionization cross sections from the total inelastic cross section, we restrict our discussions to the second term of equation (1). The imaginary part V_I of equation (2) consists the absorption potential V_{abs}, which takes into account the total loss of scattered flux into all the allowed inelastic channels. For V_{abs}, we have used the model potential of Staszewska et al. [43], which is a non-empirical, quasi-free, Pauli-blocking, dynamic absorption potential. The form of the potential is given as

$$V_{abs}(r, E_i) = -\rho(r)\sqrt{\frac{T_{loc}}{2}}\left(\frac{8\pi}{10k_F^3 E_i}\right) \times \theta(p^2 - k_F^2 - 2\Delta)(A_1 + A_2 + A_3). \quad (2)$$

The parameters A_1, A_2 and A_3 are defined as

$$A_1 = 5\frac{k_f^3}{2\Delta}, \qquad A_2 = \frac{k_f^3\left(5p^2 - 3k_f^2\right)}{\left(p^2 - k_f^2\right)^2},$$

$$A_3 = \frac{2\theta\left(2k_f^2 + 2\Delta - p^2\right)\left(2k_f^2 + 2\Delta - p^2\right)^{5/2}}{\left(p^2 - k_f^2\right)^2}. \quad (2a)$$

The local kinetic energy of the incident electron is given by

$$T_{loc} = E_i - (V_{st} + V_{ex}). \quad (3)$$

The absorption potential is a function of atomic/molecular charge density ($\rho(r)$), incident energy (E_i) and the parameter Δ of the target. It is not sensitive to long range potentials like V_{pol} and hence is neglected in local kinetic energy term of equation (3). In equation (2), $p^2 = 2E_i$, is the energy of incident electron in Hartree, $k_F = [3\pi^2\rho(r)]^{1/3}$ is the Fermi wave vector. Further $\theta(x)$ is the Heaviside unit step-function, such that $\theta(x) = 1$ for $x \geq 0$, and is zero otherwise. The dynamic functions A_1, A_2 and A_3 of equation (2) depend differently on $\rho(r)$, I, Δ and E_i. The parameter Δ determines a threshold below which $V_{abs} = 0$, and the ionization or excitation is prevented energetically. In order to include the excitations due to discrete levels at lower energy, we have considered Δ as the energy dependent parameter. So, Δ as a variable accounts for more penetration of the absorption potential in the target charge-cloud region [24,25,37,44]. Following the earlier works in this regard [24,25,37], we express Δ as a function of E_i around I as

$$\Delta(E_i) = 0.8I + \beta(E_i - I). \tag{4}$$

Here, β is obtained by requiring that $\Delta = I$ at $E_i = E_p$, where E_p is the value of E_i at which Q_{inel} attains maximum value. For $E_i > E_p$, Δ is held constant equal to ionization energy of the target as suggested in the original model of Staszewska et al. [43]. The choice of $\Delta = I$ throughout the incident energy range would not allow even excitation at $E_i \leq I$. On the other hand, if parameter Δ is much less than the ionization threshold, then V_{abs} becomes exceedingly high near the peak position.

After generating the full complex optical potential given in equation (1) for a given electron atom/molecule system, we solve the Schrödinger equation numerically with Numerov method using partial wave analysis. At low incident electron energies only few partial waves are significant, e.g. at ionization threshold of the target around 5–6 partial waves are sufficient but as the incident energy increases large number of partial waves are needed. Using these partial waves the complex phase shifts are obtained which are key ingredients to find the relevant cross sections. The total cross section then is expressed as

$$Q_T(E_i) = Q_{el}(E_i) + Q_{inel}(E_i). \tag{5}$$

The second term of this equation is the total inelastic cross section, Q_{inel}, which cannot be measured directly in experiments; it can be estimated indirectly by subtracting total integral elastic cross section from the measured grand total cross section. However, the measurable quantity of more applied interest is the total ionization cross section, Q_{ion}, which is contained in Q_{inel}. Thus, Q_{inel} can be partitioned into two major contributions, one due to the discrete electronic excitations and the other due to the continuum ionization contribution, viz.,

$$Q_{inel}(E_i) = \Sigma Q_{exc}(E_i) + Q_{ion}(E_i), \tag{6}$$

where ΣQ_{exc} is the sum over total excitation cross sections for all accessible electronic transitions. Q_{ion} is the total cross section of all allowed ionization processes induced by the incident electrons. ΣQ_{exc} arises mainly from the low-lying dipole allowed transitions. The contribution due to excitation cross sections to Q_{inel} progressively decreases compared to the ionization cross sections with increase of energy beyond the peak of ΣQ_{exc}. This is attributed to the fact that in the inelastic channel the peak of excitation cross sections occurs at lower energy compared to the peak of ionization. Accordingly, as the Q_{ion} rises ΣQ_{exc} falls beyond the peak of ΣQ_{exc}. By definition,

$$Q_{inel}(E_i) \geq Q_{ion}(E_i). \tag{7}$$

This inequality is very important and forms the basis of the CSP-ic method. In this method Q_{ion} cannot be rigorously derived from Q_{inel} but may be estimated by defining the energy dependent ratio of cross sections,

$$R(E_i) = \frac{Q_{ion}(E_i)}{Q_{inel}(E_i)} \tag{8}$$

such that, $0 < R \lesssim 1$.

As the complex potential could not be directly utilized to extract the ionization cross sections, in the CSP-ic method, we express the ratio R of equation (8) as a continuous function of energy for $E_i > I$, used in earlier studies as [19–25]

$$R(E_i) = 1 - f(U) = 1 - C_1\left(\frac{C_2}{U+a} + \frac{\ln(U)}{U}\right). \tag{9}$$

Here, U is the dimensionless variable defined by, $U = \frac{E_i}{I}$.

Equation (9) contains three parameters 'C_1', 'C_2' and 'a' which are determined by imposing three conditions on the ratio $R(E_i)$:

$$R(E_i)\begin{cases} = 0 \text{ for } E_i \leq I \\ = R_p \text{ for } E_i = E_p \\ \cong 1 \text{ for } E_i \gg E_p. \end{cases} \tag{10}$$

These conditions are understandable from the general physical arguments. Accordingly, the first condition $R = 0$ when $E_i \leq I$ is the exact condition imposed on the ratio because the ionization channel opens up only after the incident energy is greater than the ionization threshold of the target, which essentially means there is no contribution to ionization cross section below the threshold of the target. Also, the third condition is physically justified because the most important and contributing phenomenon at very high energies ($\sim 10E_P$) is the ionization process. Generally at such high energies, there are innumerable channels open for ionization. Hence the ratio will approach 1 at very high energy.

Now, R_P is the value of R at $E_i = E_P$, the energy at which the total inelastic cross section is maximum. The choice of R_P is approximate but physically justified. The peak position E_P occurs at an incident energy where the discrete excitation cross sections are on the wane, while the ionization cross section is rising fast, suggesting that the R_P value should be above 0.5 but still

below 1. We follow the general trend observed in well-known targets such as Ne, Ar, O_2, N_2, CH_4, etc. Near the peak of inelastic cross section, the contribution of the Q_{ion} is about 70–80% of the total inelastic cross section and it approaches to 100% with increase in energy. This can be basically attributed to infinitely many scattering channels offered by the continuum in contrast with a finite number of important discrete electronic excitations [37]. This competing feature of ionization versus the electronic excitations is reflected in equation (9).

Now, using equations (6) and (8) and comparing with equation (9), the function $f(U)$ can be understood as the ratio of the total discrete excitation cross section to the total inelastic cross section. The explicit form of $f(U)$ in equation (9) can be understood as follows. As E_i increases above I, the ratio R increases and approaches nearly to 1, since the ionization contribution rises and the discrete excitation term in equation (6) decreases. The discrete excitation cross sections, dominated by dipole transitions, fall off as $\ln(U)/U$ at high energies. Accordingly, the decrease of the function $f(U)$ must also go as $\ln(U)/U$ in the high incident energy. However, the first term in $f(U)$ takes care of low and intermediate E_i. The dimensionless parameters C_1, C_2, and a, involved in equation (9) are deduced using the three conditions stated in equation (10). It is obvious to note that the CSP-ic method to extract the ionization cross section does depend crucially on the choice of the value R_P.

As against the chosen value of R_p around 0.7 to 0.8 employed in the previous studies based on the CSP-ic method, in this paper, we make an attempt to provide a theoretical computation of R_P. For this purpose, we express R_P using equation (6) and equation (8) as

$$R_P = \left(1 - \frac{\Sigma Q_{exc}}{Q_{inel}}\right)_{E_i = E_P}. \tag{11}$$

Thus to get R_P, we need to compute the ratio of the total excitation cross section to the total inelastic cross section at $E_i = E_P$. Here for computing $(\Sigma Q_{exc})_{E_i=E_P}$, we need to sum up all the excitation channels from first electronic excitation (E_1) to the continuum (I) and to compute the $(Q_{inel})_{E_i=E_P}$ one has to include all the inelastic channels from E_1 to E_P. As the cross sections are continuous function of energy, we can write the ratio R_P as

$$R_P = 1 - \left(\frac{\int_{E_1}^{I} \left(\frac{dQ_{exc}}{dE}\right) dE}{\int_{E_1}^{E_P} \left(\frac{dQ_{inel}}{dE}\right) dE} \right) \tag{12}$$

and in terms of the dimensionless parameters $U_1 = E_1/I$ and $U_P = E_P/I$, R_P can be written as $1 - f(U_1, U_P)$.

Thus by knowing the energy dependence of the cross sections for the inelastic channel, the integrations of equation (12) can easily be done. In general one expects the energy dependence of the cross section as E^{-r} [45–47].

Table 2. Properties of target along with values of R_P in the CSP-ic method.

Target	E_1 (eV) [50–52]	I (eV) [53,54]	E_P (eV)	R_P
C	7.53	11.26	35	0.58
N	10.47	14.53	60	0.66
O	9.33	13.62	80	0.64
F	12.84	17.42	100	0.70
NO	6.50	9.60	60	0.64
NH_3	7.78	10.88	55	0.67

Accordingly,

$$f(U_1, U_P) = \frac{1 - U_1^r}{1 - \left(\frac{U_1}{U_P}\right)^r}. \tag{13}$$

However, it can be noted that the dominant part (elastic part) of total cross section given by Born-Bethe (BB) theory [48] tells us the E_i^{-1} dependence at low and intermediate energy range. Moreover, at the inelastic peak, the inelastic contribution matches with that of elastic contribution [49] and it provides a support to the choice of E_i^{-1} dependence at $E_i \approx E_P$. It is also seen that this relation with the exponent $r = 1$ holds true for many targets studied earlier [19–25]. Such an energy dependence on the cross sections enables us to compute the ratio R_P for any chosen target using equations (12) and (13). The computed values of R_P using equation (12) for various targets are listed in Table 2 along with their target properties. Here the first electronic excitation energy of the target is taken as an average of the corresponding electron orbital states of the target.

It is found that the computed R_P values in most of the cases studied here lie in the range 0.58 to 0.7. Though in most of the cases we get the estimated value of R_P below 0.7, we have been able to provide a physical basis in support of the choice of R_P at the peak of the inelastic cross section. We employ this new theoretically estimated value of R_P and compute the ionization cross sections for some of the few atomic and simple molecular targets listed in Table 2. The results are plotted in the respective graphs and compared with the experimental as well as with other model calculations. Thus in this paper we have improved the CSP-ic method by providing the much needed theoretical support to computation of the parameter R_P.

3 Results and discussion

The theoretical approach of SCOP along with the present improved CSP-ic method (ICSP-ic) outlined above offers the determination of the total inelastic cross sections, Q_{inel} and total ionization cross sections, Q_{ion} along with a useful estimate on electronic excitations in terms of the summed cross section ΣQ_{exc}. In the present paper, we have taken varied atoms and molecules and computed the total ionization cross sections using the newly computed value of R_P vide equation (12).

Table 3. Total ionization cross sections, Q_{ion} (Å^2) for C, N, O, F, NO and NH_3. Maximum values of the cross section are shown in the bold print.

E_i (eV)	C	N	O	F	NO	NH_3
15	0.49	0.01	0.02	—	0.34	0.28
20	1.12	0.23	0.20	0.03	0.94	0.89
30	1.83	0.75	0.64	0.27	1.96	1.94
40	2.12	1.12	0.93	0.52	2.61	2.54
50	2.23	1.34	1.10	0.69	3.01	2.85
60	**2.25**	1.47	1.19	0.81	3.25	3.03
70	**2.25**	1.54	1.24	0.89	3.37	3.11
80	2.23	1.58	1.28	0.94	3.44	3.12
90	2.19	**1.59**	1.30	0.97	**3.48**	**3.13**
100	2.13	**1.59**	**1.31**	**0.99**	**3.48**	3.10
200	1.59	1.33	1.22	**0.99**	3.21	2.48
300	1.25	1.08	1.04	0.89	2.81	2.00
400	1.03	0.90	0.90	0.78	2.49	1.67
500	0.88	0.77	0.79	0.69	2.23	1.44
600	0.77	0.68	0.71	0.62	2.02	1.26
700	0.68	0.61	0.64	0.56	1.84	1.13
800	0.62	0.55	0.59	0.51	1.70	1.02
900	0.56	0.50	0.54	0.47	1.57	0.92
1000	0.52	0.46	0.50	0.44	1.46	0.85
2000	0.29	0.26	0.30	0.26	0.85	0.44

The dependence of ionization cross sections as function of incident energy for C, N, O, F along with NO and NH_3 from threshold of the target to 2 keV are shown in Figures 1–6 respectively. The present results of the total ionization cross sections based on the ICSP-ic method for all these targets are also tabulated in Table 3 for ready reference of the numerical values.

Figure 1 shows the comparison of total ionization cross sections for e–C scattering with other available experimental and theoretical data. Brook et al. [7] have reported ionization measurements for e–C scattering using crossed beam method in which fast beam of atoms are produced by charge capture of 2 and 4 keV ions in a gas target over the energy 7 to 1000 eV. The measured data of Brook et al. [7] are overall in good agreement with the present data throughout the energy range reported by them. The theoretical data of Kim and Desclaux [29,30] and recommended data of Bell et al. [32] are also in good accord with present data. The theoretical data reported by McGuire [31] shows a leftward shift in their peak and are higher compared to all reported values near and below the peak.

Figure 2 shows the comparison of total ionization cross section for e–N scattering with available comparisons. Experimental data of Brook et al. [7] are in excellent agreement with present data beyond 30 eV below which present data are slightly lower than the experimental values. The theoretical data of Kim and Desclaux [29,30] and Rong-Mei et al. [33] are in good agreement with present data except towards the peak, where they are lower compared to the present data. The theoretical data of McGuire [31] are exceptionally high compared to all reported values at the peak. However beyond 250 eV they are in excellent agreement with present data.

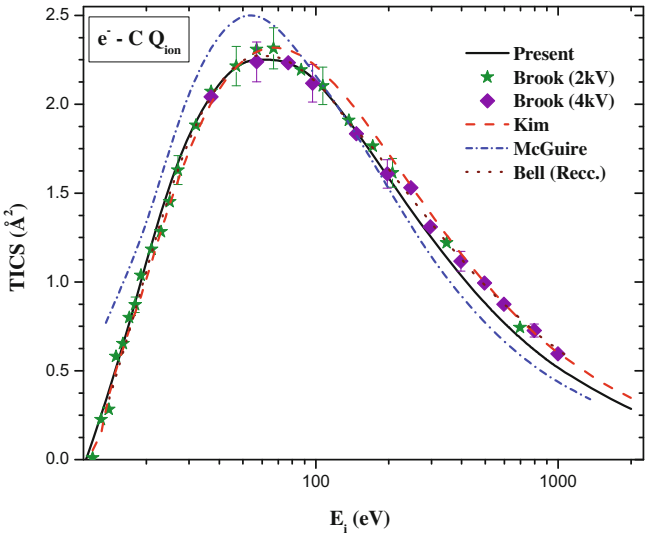

Fig. 1. (Color online) Total ionization cross sections, Q_{ion}, for e–C scattering in Å^2. Solid line: present results with ICSP-ic method. Dashed line: Kim and Desclaux [29,30]. Dashed dot line: McGuire [31]. Short Dashed line: Bell et al. [32]. Stars: Brook et al. (2 keV) [7]. Squares: Brook et al. (4 keV) [7].

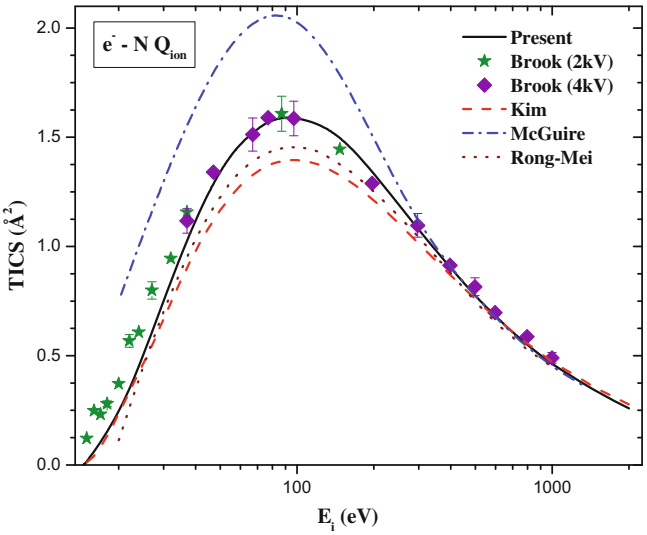

Fig. 2. (Color online) Total ionization cross sections, Q_{ion}, for e–N scattering in Å^2. Solid line: present results with ICSP-ic method. Dashed line: Kim and Desclaux [29,30]. Dashed dot line: McGuire [31]. Dotted line: Rong-Mei et al. [33]. Stars: Brook et al. (2 keV) [7]. Squares: Brook et al. (4 keV) [7].

In Figure 3, we have compared our total ionization data for e–O scattering with other available theoretical and experimental data. There is excellent agreement of the present data with experimental measurements of Brook et al. [7], Zipf [9] and recommended data of Bell et al. [32] throughout the energy range. Present data finds good accord with the experimental data of Thomson et al. [8] and theoretical data of Kim and Desclaux [29,30] at all energies except at the peak where present data is slightly lower. Theoretical data of McGuire [31] are in very good agreement with present data till 50 eV beyond which they

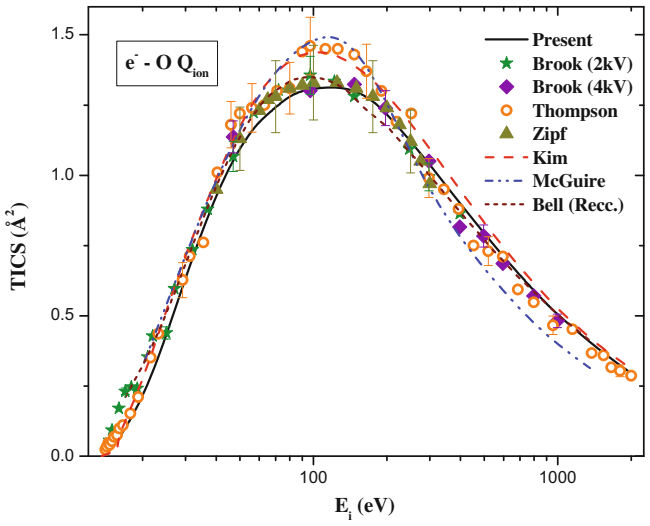

Fig. 3. (Color online) Total ionization cross sections, Q_{ion}, for e–O scattering in Å^2. Solid line: present results with ICSP-ic method. Dashed line: Kim and Desclaux [29,30]. Dashed dot line: McGuire [31]. Short Dashed line: Bell et al. [32]. Stars: Brook et al. (2kV) [7]. Squares: Brook et al. (4 keV) [7]. Open circles: Thompson et al. [8]. Triangles: Zipf [9].

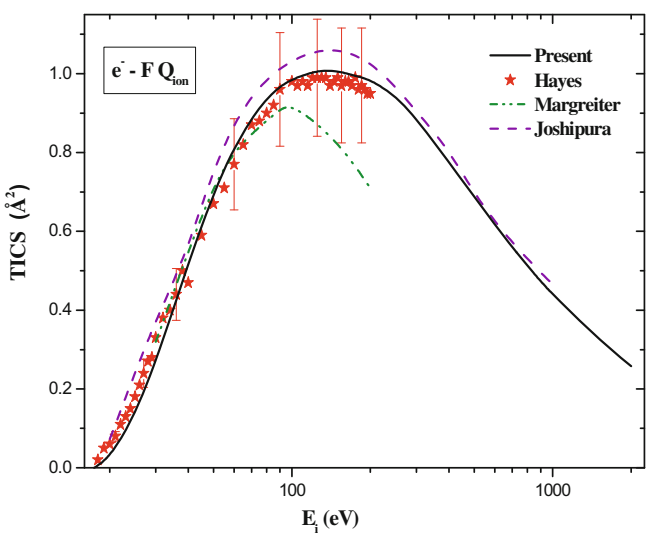

Fig. 4. (Color online) Total ionization cross sections, Q_{ion}, for e–F scattering in Å^2. Solid line: present results with ICSP-ic method. Dashed dot line: Margreiter et al. [34]. Dashed line: Joshipura and Limbachiya [35]. Stars: Hayes et al. [4].

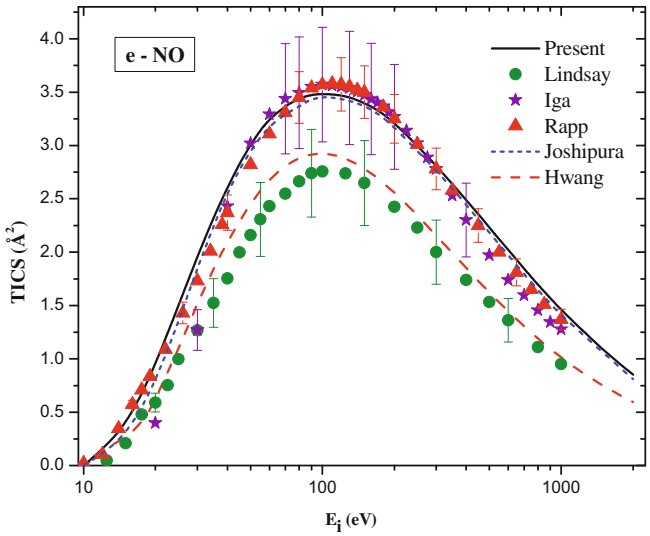

Fig. 5. (Color online) Total ionization cross sections, Q_{ion}, for e–NO scattering in Å^2. Solid line: present results with ICSP-ic method. Short dashed line: Joshipura et al. [37]. Dashed line: Hwang et al. [29,36]. Stars: Iga et al. [10]. Filled circles: Lindsay et al. [11]. Solid up triangles: Rapp and Englander-Golden [5].

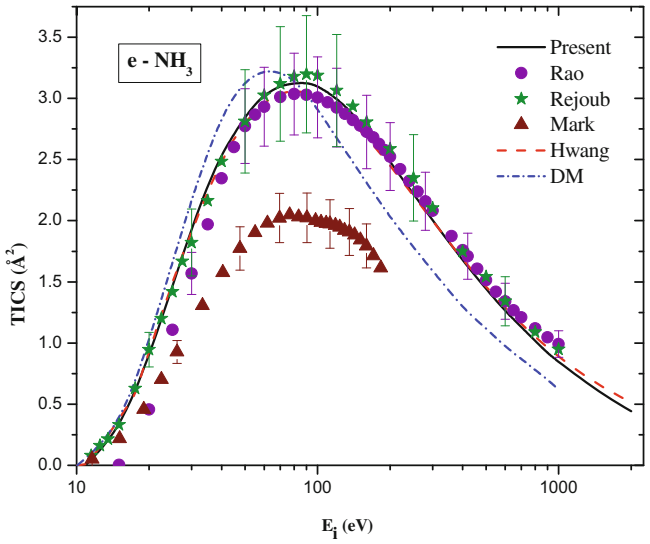

Fig. 6. (Color online) Total ionization cross sections, Q_{ion}, for e–NH_3 scattering in Å^2. Solid line: present results with ICSP-ic method. Dashed line: Hwang et al. [29,36]. Dashed dot line: Deutsch et al. [38]. Filled circles: Rao and Srivastava [3]. Stars: Rejoub et al. [13]. Solid up triangles: Märk et al. [6].

are slightly higher than the present results at the peak region and suddenly drop after the peak compared to all other reported data.

Figure 4 shows comparison of present total ionization cross sections for e–F scattering with available data. Flourine being a reactive atom, lesser data sets are available for comparison. The present data are in very good agreement with experimental data of Hayes et al. [4] throughout the range of energy specified by them. The theoretical data of Joshipura and Limbachiya [35] are slightly higher compared to all reported values. The theoretical values of Margreiter et al. [34] are in good accord with present data till 80 eV above which they suddenly decrease.

Figure 5 depicts the comparison of total ionization cross sections for e–NO scattering which is also studied

using the ICSP-ic method from threshold to 2 keV. The present results are slightly higher than the theoretical results of Joshipura et al. [37]. It is evident from the figure that present results compare excellently well with experimental results of Rapp and Englander-Golden [5] throughout the specified energy range. In addition the present results are in very well accord with experimental results of Iga et al. [10] except at high energies where they are slightly higher but falls within the experimental uncertainty which is around 15%. The experimental results of Lindsay et al. [11] and theoretical results of Hwang et al. [29,36] are much lower than the present ICSP-ic results and experimental results of Iga et al. [10] throughout the energy range. However the shape and peak of the curve remains the same for all the reported data.

Finally Figure 6 shows the comparison of ionization cross sections for e–NH_3 scattering, studied using ICSP-ic method from threshold to 2 keV. The present results are in excellent accord with the experimental results of Rao and Srivastava [3] and Rejoub et al. [13] and theoretical values of Hwang et al. [29,36] throughout the range of energy. The theoretical values of Deutsch et al. [38] are good at low energies but the peak is shifted towards the left and so the whole curve is shifted left compared to other reported data sets [3,6,13,29,36]. The experimental data of Märk et al. [6] are very low, almost 50% compared to all reported values; however the peak is almost at the same energy as that of the present data.

As expected it is observed that peak of the ionization cross section shifts towards higher energy as ionization threshold increases. For instance for C (I = 11.26 eV) peak at 60 eV, O (I = 13.62 eV) peak at 90 eV, N (I = 14.53 eV) peak at 125 eV and F (I = 17.42 eV) peak at 150 eV. It is observed that lower the ionization threshold higher is the value of ionization cross sections for e.g. C (I = 11.26 eV) the highest value of cross section is 2.25 Å^2 and for F (I = 17.42 eV) the highest value of cross section is 0.99 Å^2.

The general comparison of the ionization cross section curves for NH_3 and NO again reflects the same observation as seen earlier for all the investigated targets that both these molecules have peak around 100 eV as their ionization thresholds are also nearer i.e. 10.88 eV for NH_3 and 9.6 eV for NO. Also the peak value of the ionization cross section is function of size of the target, for instance 3.13 Å^2 for NH_3 (10 electrons) and 3.48 Å^2 for NO (15 electrons).

It is to be noted that for all the targets investigated here the nature of the ionization cross section is similar to the expected behavior in which the ionization cross section increases with increase in the incident energy up to the peak. This is attributed to the fact that with increase in the incident energy the electron can penetrate more within the target and hence the interaction increases progressively. But beyond the peak, though the energy of the projectile is increased, the effective time it spends with the target decreases, which eventually causes the decrease in the value of ionization cross section.

4 Conclusion

The complex scattering potential–ionization contribution (CSP-ic) formalism is used to derive the total ionization cross section and has been tested successfully for a large number of atomic and molecular targets [19–25]. Though successful, it involves choice of R_P, which was heuristically chosen for different targets. Here we have made an attempt to derive this ratio, R_P using the basic properties of the target such as first electronic excitation energy (E_1) and ionization threshold (I).

The modification introduced in the present study is noteworthy from Table 2 that the values of R_P evaluated in the present study through equation (13) fall around 0.58 to 0.7 as against 0.7 to 0.8 considered earlier [19–25]. With this improved CSP-ic (ICSP-ic) method we have computed total ionization cross sections for few atoms (C, N, O, and F) and two molecules NH_3 and NO. It can be seen in Figures 1–6 that the present data for the ionization cross sections are in better agreement with number of experimental and theoretical data for all the targets studied here. This shows the consistency of the present ICSP-ic formalism. Also, the present method employed here provides an estimate of electronic excitations in relation to ionization cross sections in a particular target. It is to be noted that the present method needs the first electronic excitation energy (E_1) and the ionization threshold (I) as inputs for the calculation of R_p. We note that in view of the approximations involved in the CSP-ic method, though no definitive claims can be made, by and large our results fall within the experimental error limits in most of the cases.

The other noteworthy observation is that the incident energy at which peak of the ionization cross section occurs is dependent on the ionization threshold of the target. The peak shifts towards the higher energy side with increase in the ionization threshold of the target. It is also observed and confirms the established fact that the cross section increases with increase in the geometric size of the target. Finally, we have been able to provide the much needed physical basis for the CSP-ic method.

MVK is grateful to the University Grants Commission, New Delhi, for a Major Research Project under which part of this work is carried out.

References

1. L.G. Christophorou, J.K. Olthoff, *Fundamental Electron Interactions with Plasma Processing Gases* (Kluwer, Dordrecht Plenum, New York, 2004)
2. N.J. Mason, J.M. Gingell, N.C. Jones, L. Kaminski, Philos. Trans. R. Soc. Lond. A **357**, 1175 (1999), and references therein
3. M.V.V.S. Rao, S.K. Srivastava, J. Phys. B: At. Mol. Opt. Phys. **25**, 2175 (1992)
4. T.R. Hayes, R.C. Wetzel, R.C. Freund, Phys. Rev. A **35**, 578 (1987)

5. D. Rapp, P. Englander-Golden, J. Chem. Phys. **43**, 1464 (1965)
6. T.D. Märk, F. Egger, M. Cheret, J. Chem. Phys. **67**, 3795 (1977)
7. E. Brook, M.F.A. Harrison, A.C.H. Smith, J. Phys. B: At. Mol. Opt. Phys. **11**, 3115 (1978)
8. W.R. Thompson, M.B. Shah, H.B. Gilbody, J. Phys. B: At. Mol. Opt. Phys. **28**, 1321 (1995)
9. E.C. Zipf, Planet. Space Sci. **33**, 1303 (1985)
10. I. Iga, M.V.V.S. Rao, S.K. Srivastava, J. Geophys. Res. **101**, 9261 (1996)
11. B.G. Lindsay, M. A. Mangan, H.C. Straub, R.F. Stebbings, J. Chem. Phys. **112**, 9404 (2000)
12. J. Lopez, V. Tarnovsky, M. Gutkin, K. Becker, Int. J. Mass Spectrom. Ion Proc. **225**, 25 (2003)
13. R. Rejoub, B.G. Lindsay, R.F. Stebbings, J. Chem. Phys. **115**, 5053 (2001)
14. H. Deutsch, K. Becker, T.D. Märk, Int. J. Mass Spectrom. Ion Proc. **167/168**, 503 (1997)
15. I. Bray, D.V. Fursa, Phys. Rev. A **54**, 2991 (1996)
16. M. Bobeldijk, W.J. van der Zande, P.G. Kistemaker, Chem. Phys. **179**, 125 (1994)
17. S.P. Khare, W.J. Meath, J. Phys. B: At. Mol. Opt. Phys. **20**, 2101 (1987)
18. Y.-K. Kim, M.E. Rudd, Phys. Rev. A **50**, 3954 (1994)
19. K.N. Joshipura, B.K. Antony, M. Vinodkumar, J. Phys. B: At. Mol. Opt. Phys. **35**, 4211 (2002)
20. K.N. Joshipura, M. Vinodkumar, B.K. Antony, N.J. Mason, Eur. Phys. J. D **23**, 81 (2003)
21. K.N. Joshipura, M. Vinodkumar, C.G. Limbachiya, B.K. Antony, Phys. Rev. A **69**, 022705 (2004)
22. M. Vinodkumar, K.N. Joshipura, C. Limbachiya, N. Mason, Phys. Rev. A **74**, 022721 (2006)
23. M. Vinodkumar, C. Limbachiya, B. Antony, K.N. Joshipura, J. Phys. B: At. Mol. Opt. Phys. **40**, 3259 (2007)
24. M. Vinodkumar, C. Limbachiya, K. Korot, K.N. Joshipura, Eur. Phys. J. D **48**, 333 (2008)
25. M. Vinodkumar, C. Limbachiya, K. Korot, K.N. Joshipura, N. Mason, Int. J. Mass Spectrom. Ion Proc. **273**, 145 (2008)
26. M.F.A. Harrison, *Atomic and Molecular Data for Fusion* (International Atomic Energy Agency, Vienna, Technical Report IAEA-199, 1977), pp. 81–113
27. L.R. Arana, N. de Mas, R. Schmidt, A.J. Franz, M.A. Schmidt, K.F. Jensen, J. Micromech. Microeng. **17**, 384 (2007)
28. M. Imami, W.L. Borst, J. Chem. Phys. **63**, 3602 (1975)
29. From: http://physics.nist.gov/PhysRefData/Ionization/
30. Y.-K. Kim, J.-P. Desclaux, Phys. Rev. A **66**, 012708 (2002)
31. E.J. McGuire, Phys. Rev. A **3**, 267 (1971)
32. K.L. Bell, H.B. Gilbody, J.G. Hughes, A.E. Kingston, F.J. Smith, J. Phys. Chem. Ref. Data **12**, 981 (1983)
33. Yu Rong-Mei , Zhou Ya-Jun , Wang Yang, Jiao Li-Guang , Chin. Phys. Lett. **23**, 3256 (2006)
34. D. Margreiter, H. Deustch, T.D. Märk, Int. J. Mass Spectrom. Ion Proc. **139**, 127 (1994)
35. K.N. Joshipura, C.G. Limbachiya, Int. J. Mass Spectrom. Ion Proc. **216**, 239 (2002)
36. W. Hwang, Y.-K. Kim, M.E. Rudd, J. Chem. Phys. **104**, 2957 (1996)
37. K.N. Joshipura, S. Gangopadhyay, B.G. Vaishnav, J. Phys. B: At. Mol. Opt. Phys. **40**, 199 (2007)
38. H. Deutsch, K. Becker, S. Matt, T.D. Märk, Int. J. Mass Spectrom. Ion Proc. **197**, 37 (2000)
39. A. Jain, J. Phys. B **21**, 905 (1988)
40. C.F. Bunge, J.A. Barrientos, A.V. Bunge, At. Data Nucl. Data Tables **53**, 113 (1993)
41. I. Gradashteyn, I.M. Ryzhik, *Tables of Integrals, Series and Products* (Associated Press, New York, 1980)
42. A. Jain, K.L. Baluja, Phys. Rev. A **45**, 202 (1992)
43. G. Staszewska, D.W. Schwenke, D. Thirumalai, D.G. Truhlar, Phys. Rev. A **28**, 2740 (1983)
44. F. Blanco, G. Garcia, Phys. Rev. A **67**, 022701 (2003)
45. G. Garcia, F. Manero, Chem. Phys. Lett. **280**, 419 (1997)
46. A. Zecca, G.P. Karwasz, R.S. Brusa, Phys. Rev. A **46**, 3877 (1992)
47. C. Szmystkowski, A.M. Krzysztofowicz, J. Phys. B: At. Mol. Opt. Phys. **28**, 4291 (1995)
48. G. Garcia, F. Blanco, Phys. Rev. A **62**, 044702 (2000)
49. J. Joachain, *Quantum Collision Theory* (Amsterdam, North-Holland, 1983)
50. From: http://physics.nist.gov/PhysRefData/ASD/levels_form.html
51. D.L. Albritton, A.L. Schmeltekopf, R.N. Zare, J. Chem. Phys. **71**, 3271 (1979)
52. H. Munjal, K.L. Baluja, Phys. Rev. A **74**, 032712 (2006)
53. D.R. Lidez, *CRC Handbook of Physics and Chemistry*, 74th edn. (Chemical Rubber Company, Boca Raton, FL, 1993-94)
54. From: http://srdata.nist.gov/cccbdb/